Submitted to ApJ Letters
Preprint typeset using LaTeX style emulateapj v. 5/2/11

arXiv:1304.2395v1 [astro-ph.CO] 8 Apr 2013

THE STRUCTURAL EVOLUTION OF MILKY WAY-LIKE STAR FORMING GALAXIES SINCE $z \sim 1.3$*

Shannon G. Patel[1], Mattia Fumagalli[1], Marijn Franx[1], Pieter G. van Dokkum[2], Arjen van der Wel[3], Joel Leja[2], Ivo Labbé[1], Gabriel Brammer[4], Rosalind E. Skelton[2], Ivelina Momcheva[2], Katherine E. Whitaker[5], Britt Lundgren[6], Adam Muzzin[1], Ryan F. Quadri[7], Erica June Nelson[2], David A. Wake[6], Hans-Walter Rix[3]
[1]Leiden Observatory, Leiden University, P.O. Box 9513, NL-2300 AA Leiden, Netherlands; patel@strw.leidenuniv.nl
[2]Department of Astronomy, Yale University, New Haven, CT 06511, USA
[3]Max-Planck-Institut fur extraterrestrische Physik, Giessenbachstrasse, D-85748 Garching, Germany
[4]European Southern Observatory, Alonson de Cordova 3107, Casilla 19001, Vitacura, Santiago, Chile
[5]Astrophysics Science Division, Goddard Space Center, Greenbelt, MD 20771, USA
[6]Department of Astronomy, University of Wisconsin-Madison, Madison,WI 53706, USA
[7]Observatories of the Carnegie Institution of Washington, Pasadena, CA 91101, USA

Submitted to ApJ Letters

ABSTRACT

We follow the structural evolution of star forming galaxies (SFGs) like the Milky Way by selecting progenitors to $z \sim 1.3$ based on the stellar mass growth inferred from the evolution of the star forming sequence. We select our sample from the 3D-HST survey, which utilizes spectroscopy from the *HST* WFC3 G141 near-IR grism and enables precise redshift measurements for our sample of SFGs. Structural properties are obtained from Sérsic profile fits to CANDELS WFC3 imaging. The progenitors of $z = 0$ SFGs with stellar mass $M = 10^{10.5}\ M_{\odot}$ are ~ 2 times less massive at $z \sim 1$. This late-time stellar mass assembly is consistent with recent studies that employ abundance matching techniques. The descendant SFGs at $z \sim 0$ have grown in half-light radius by a factor of ~ 1.4 since $z \sim 1$. The half-light radius grows with stellar mass as $r_e \propto M^{0.29}$. While most of the stellar mass is clearly assembling at large radii, the mass surface density profiles reveal ongoing mass growth also in the central regions where bulges and pseudobulges are common features in present day late-type galaxies. Some portion of this growth in the central regions is due to star formation as recent observations of Hα maps for SFGs at $z \sim 1$ are found to be extended but centrally peaked. Connecting our lookback study with galactic archeology, we find the stellar mass surface density at $R = 8$ kpc to have increased by a factor of ~ 2 since $z \sim 1$, in good agreement with measurements derived for the solar neighborhood of the Milky Way.

Subject headings: galaxies: structure — galaxies: evolution — galaxies: formation

1. INTRODUCTION

The formation of late-type star forming galaxies (SFGs) like the Milky Way has been studied through several complementary approaches in order to understand the assembly of the disk and bulge. On the observational front, detailed studies of the ages, metallicities, and kinematics of stellar populations within the Milky Way itself afford a unique vantage point for viewing the assembly of such late-type galaxies. This extremely informative approach is limited in completeness and sample size and must contend with a reconstruction of the global star formation and structural assembly history, which is a complex task (see, e.g., Roškar et al. 2008; Rix & Bovy 2013, and references therein). On the theoretical front, the formation of Milky Way-like SFGs has posed a challenge for the numerous simulations that aim to produce a structurally realistic analog at $z \sim 0$ with a disk and an embedded bulge or pseudobulge (Scannapieco et al. 2012). In particular, this latter work shows how many of the simulations form massive bulges at early times, lack prominent disks at late times, and produce widely varying physical properties for the descendant galaxy at $z = 0$. This largely reflects the challenge of correctly modeling the "sub-grid" physical processes that impact the baryons. Recently, however, there has been some success among a few simulations in producing late-type SFGs like the Milk Way within specific halos (e.g., Guedes et al. 2011; Stinson et al. 2013).

In this Letter, we employ a lookback study that complements the galactic archeology and theoretical methods above in order to understand how late-type SFGs like the Milky Way were assembled. We select star forming progenitors using the stellar mass growth inferred from the evolution of the star forming sequence and analyze their structural evolution using *HST* imaging. This method for computing the mass growth of SFGs has been discussed in detail by Leitner (2012) and complements other studies which connect progenitors and descendants using number densities (van Dokkum et al. 2010; Patel et al. 2013). Given the distinct formation history of SFGs from quiescent galaxies (QGs), we use the former method here as it directly traces the star forming progenitors of galaxies like the Milky Way. In van Dokkum et al. (2013), we use the number density approach to study progenitors of galaxies of all types with the mass of the Milky Way.

We assume a cosmology with $H_0 = 70$ km s^{-1} Mpc^{-1}, $\Omega_M = 0.30$, and $\Omega_\Lambda = 0.70$. Stellar masses are based on a Chabrier IMF (Chabrier 2003). Magnitudes are in the AB system.

---

* Based on observations made with the NASA/ESA Hubble Space Telescope, obtained at the Space Telescope Science Institute. STScI is operated by the Association of Universities for Research in Astronomy, Inc. under NASA contract NAS 5-26555.

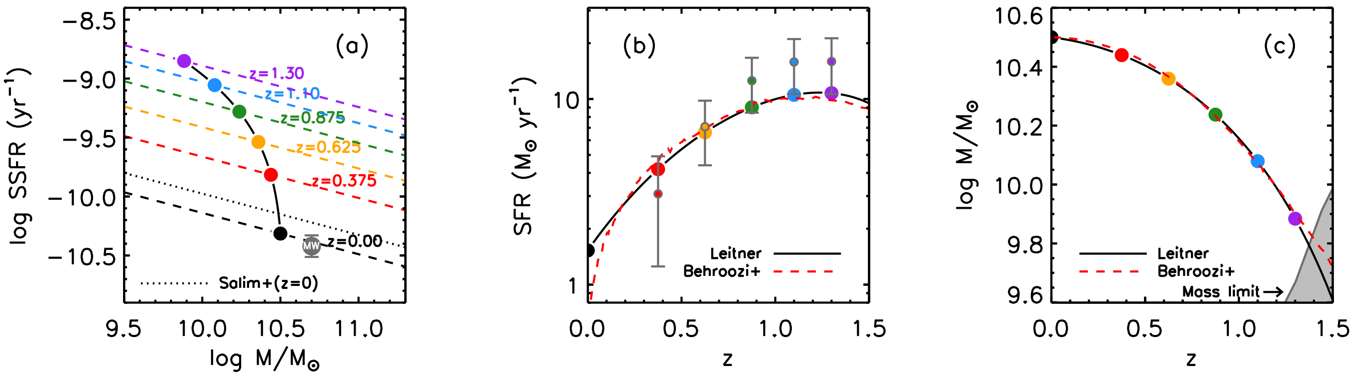

Figure 1. (a) Evolution of SFGs in the SSFR-mass plane with final mass at $z \sim 0$ of $M = 10^{10.5}\ M_\odot$ as computed by Leitner (2012) using the SSFR-mass relations at different redshifts (dashed lines) from Karim et al. (2011). At a given redshift, new stellar mass is added according to the position of the SFG on the star forming sequence and mass loss from stellar evolution is also accounted for. The slight offset between the extrapolated $z = 0$ relation from that of Salim et al. (2007) does not impact our results (see text). The Milky Way (gray circle) lies within the observational scatter of the $z = 0$ relation. (b) SFH of the SFGs tracked in panel (a). The data points with error bars represent IR+UV SFRs for a subset of our sample with deep MIPS: there is good general agreement with the radio based SFRs from Karim et al. (2011). (c) Mass growth history of the SFGs tracked in panel (a). We select galaxies at the indicated masses and redshifts in this Letter. Since $z = 1$, the SFGs grow in stellar mass by a factor of ~ 2. For comparison, the SFH and mass growth for galaxies with the same final mass from Behroozi et al. (2012) is shown by the dashed red line. There is excellent agreement between the observationally motivated method used here and the more theoretically motivated method of Behroozi et al. (2012).

2. DATA AND ANALYSIS

We employ data from the 3D-HST survey ($v2.1$) to carry out our analysis. The observations and data reduction procedures are explained in detail in Brammer et al. (2012) and Skelton et al. (in prep.). The *HST* WFC3 G141 near-IR grism observations are the centerpiece of 3D-HST and cover the CANDELS fields. In this work, we use the three fields with currently available WFC3 based structural parameters from the literature: COSMOS, GOODS-S, and UDS. Grism redshifts were measured using a modified version of EAZY (Brammer et al. 2008). The procedure fits template SEDs to both the photometry and grism spectroscopy, enabling precise redshift measurements for our sample of SFGs at high redshift.

Stellar masses were measured with FAST (Kriek et al. 2009). We determine the stellar mass limit at our highest redshifts ($z = 1.4$) to be $M \sim 10^{9.8}\ M_\odot$ (see Figure 1(c)) using a similar technique to that of Marchesini et al. (2009). This conservative limit accounts for galaxies with high M/L such as reddened SFGs. Rest-frame $U-V$ and $V-J$ colors were measured with EAZY in order to distinguish SFGs from QGs (Section 3.2).

Structural properties were obtained from van der Wel et al. (2012) who used GALFIT (Peng et al. 2002) to fit Sérsic profiles to the CANDELS *HST* WFC3 J_{125} and H_{160} imaging (Grogin et al. 2011; Koekemoer et al. 2011). The effective radii reported here are circularized. The J_{125} imaging is used at $0.25 < z < 1$ while the H_{160} imaging is used at $1 < z < 1.4$, with our median galaxy sampling rest-frame $\sim$ 7100 Å. The PSF FWHM/2 of the H_{160} imaging is $\sim 0\farcs09$, corresponding to a physical radius at our highest redshifts of ~ 0.8 kpc.

We employ an SDSS reference sample at $z = 0.05$ using stellar masses and SFRs from the MPA/JHU catalogs (Brinchmann et al. 2004) and i-band Sérsic fits from the NYU-VAGC (Blanton et al. 2003, 2005).

3. SELECTION

3.1. *Stellar Mass Growth History from an Evolving Star Forming Sequence*

In this work, we trace the formation of SFGs with a final mass slightly below that of the Milky Way (~ 0.2 dex) so that we can compare various properties to galaxies of the same final mass from other works that employ different progenitor-descendant linking methods (e.g., Behroozi et al. 2012). We note however that we arrive at similar qualitative conclusions when tracing progenitors of Milky Way-mass SFGs.

Selecting progenitors of $z \sim 0$ SFGs requires knowledge of their mass growth history so that one can select galaxies of the proper progenitor mass at a given redshift. For galaxies that assemble most of their stars from in-situ star formation, one can infer the mass growth from the evolution in the SFR-mass relation (or SSFR-mass). The Milky Way, with a stellar mass of $M \sim 5 \times 10^{10}\ M_\odot$ (Hammer et al. 2007) and a SFR of $1.9 \pm 0.4\ M_\odot\ \mathrm{yr}^{-1}$ (Chomiuk & Povich 2011), falls within the observational scatter of the SSFR-mass relation of Salim et al. (2007, their Eq. 11, corrected for evolution to $z = 0$ assuming Equation 1 here; see Figure 1(a)). This star-forming sequence has been extensively studied to high redshifts (e.g., Noeske et al. 2007; Karim et al. 2011; Whitaker et al. 2012; Fumagalli et al. 2012). The method for determining the mass growth from this relation is simple: for a given redshift interval, new stellar mass is added to the existing mass based on the location of a galaxy in the SSFR-mass plane and mass loss from stellar evolution is accounted for from simple stellar population models. The assumption that most nearby SFGs were star forming at high redshift is supported by the small scatter about the SSFR-mass relation ($\sigma \sim 0.17$ dex after accounting for observational uncertainties; Whitaker et al. 2012) as well as by the vastly different structural properties between SFGs and QGs (e.g., Franx et al. 2008).

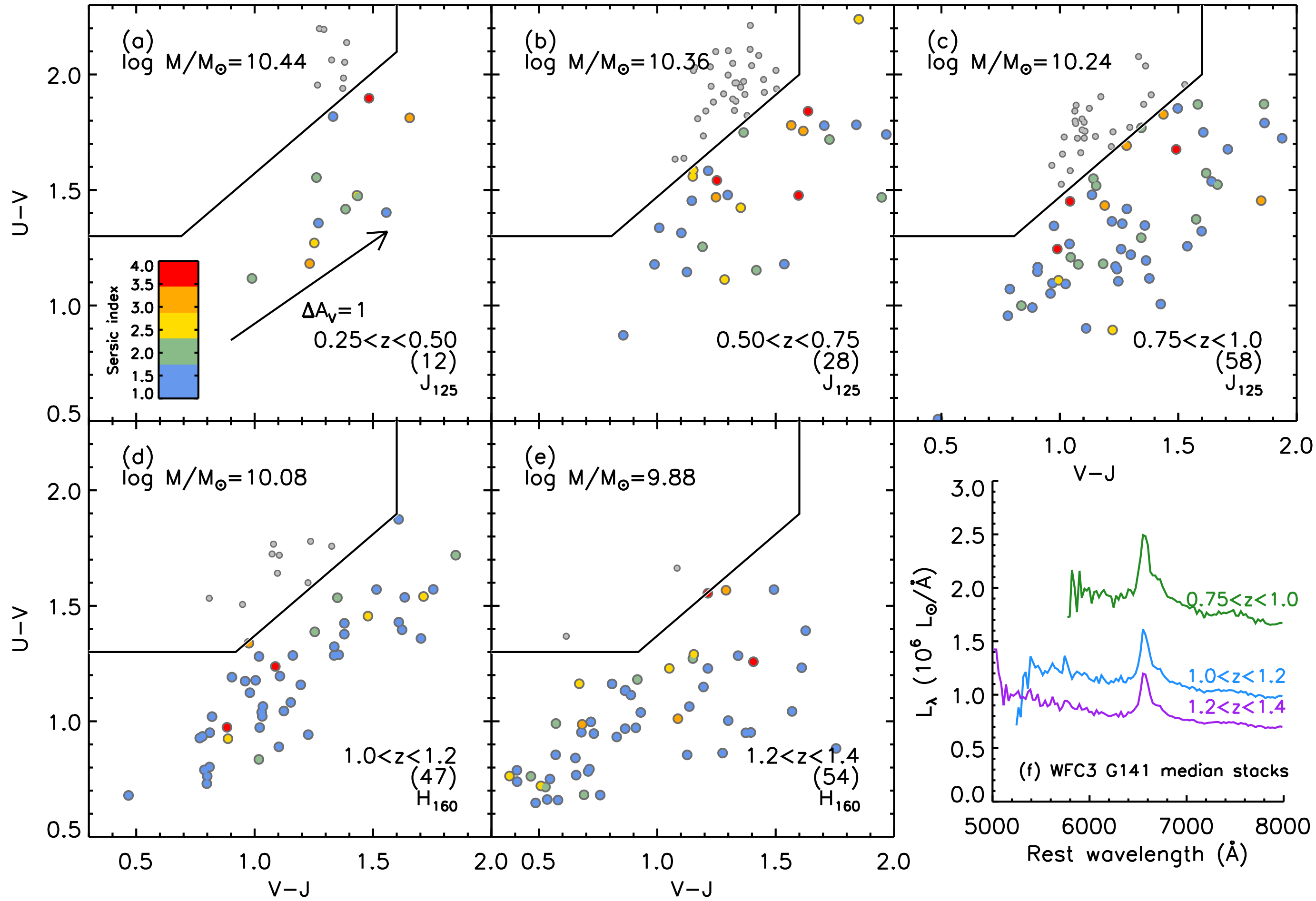

Figure 2. (a)-(e) Rest-frame $U-V$ versus $V-J$ at different redshifts, with galaxies selected to have the progenitor mass (± 0.1 dex) from Figure 1(c). The Williams et al. (2009) boundary separating QGs from SFGs (bottom right) is used to select the latter. These SFGs are color-coded according to their Sérsic indices. (f) WFC3 G141 median stacked spectra of SFGs for redshift bins with observable Hα.

In this work, we use the mass growth computed by Leitner (2012), who derived it from the SSFR-mass relations of Karim et al. (2011). Figure 1(a) shows SSFR-mass relations at different redshifts (dashed lines) measured by Karim et al. (2011) from 1.4 GHz radio stacking. They employ the parameterization:

$$SSFR \propto M^{\beta}(1+z)^{n} \quad (1)$$

where $\beta = -0.35$ and $n = 3.45$. Though the $z = 0$ relation based on Equation 1 is an extrapolation of the Karim et al. (2011) data, its slight difference from lower redshift observations (e.g., Salim et al. 2007) does not significantly impact the mass growth at these late times. The track shown in Figure 1(a) (black curve) indicates the trajectory in the SSFR-mass plane for the SFGs selected for study in this work with final mass at $z = 0$ of $M = 10^{10.5}$ $M_\odot$. The corresponding SFH is shown in panel (b) and the mass growth with redshift in panel (c). The points with error bars (including a 30% systematic uncertainty) in panel (b) indicate the median SFR (IR+UV) of our sample in the GOODS fields (i.e., deep MIPS) for our UVJ-selected (see below) SFGs at the corresponding redshifts and masses from panel (c). While SFR estimates can vary due to systematics between different tracers (e.g., Wuyts et al. 2011; Leitner 2012) there is good general agreement between our SFR measurements and those of Karim et al. (2011). The dashed red curves in panels (b) and (c) show the corresponding result for the same final mass galaxy from Behroozi et al. (2012) whose results were derived from a more theoretical approach that combined merger trees from dark matter simulations with observational constraints. The latter is consistent with our observationally motivated method.

The results above suggest significant stellar mass assembly in our SFGs below $z < 1$ (factor of ~ 2.2). Late assembly at $z < 1$ is also found by other abundance matching works (e.g., Moster et al. 2013). SFHs of the Milky Way disk derived from stellar properties also suggest significant late time assembly (e.g., Rocha-Pinto et al. 2000; Aumer & Binney 2009). Finally, hydrodynamical simulations also appear to favor late time assembly for Milky Way-like galaxies given that earlier formation fails to produce a prominent stellar disk (Scannapieco et al. 2012).

3.2. *Selection of Star Forming Progenitors to $z \sim 1.3$*

Given the observational scatter about the SSFR-Mass relation, in practice we select all SFGs in a given redshift and mass bin. Figure 2 shows rest-frame $U-V$ vs. $V-J$ diagrams for galaxies in narrow mass bins

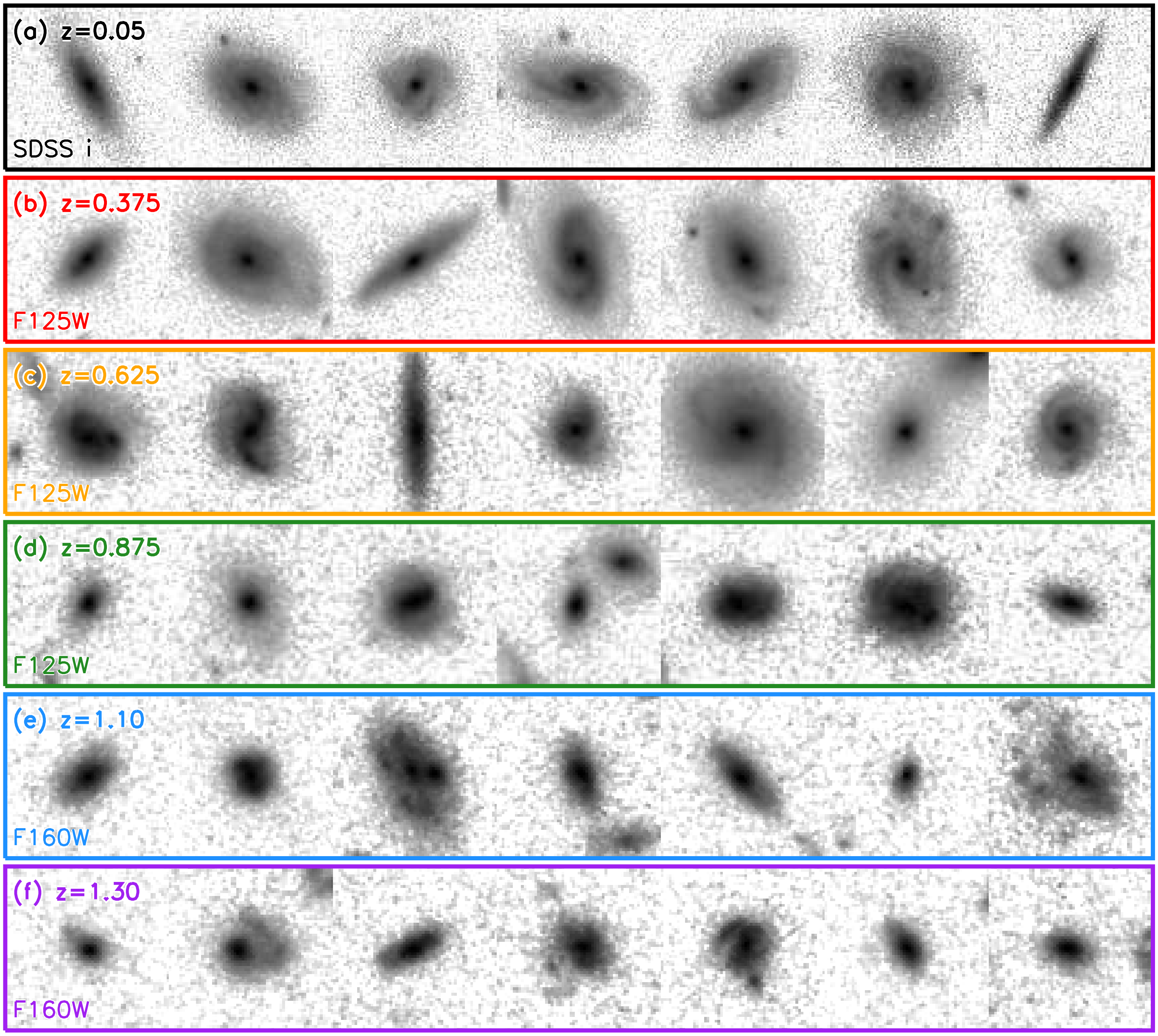

Figure 3. Example SDSS *i*-band and *HST* WFC3 postage stamps for progenitors of SFGs with a final mass at $z = 0$ of $M = 10^{10.5}\ M_\odot$. Each stamp is $\sim$ 30 kpc on a side. The median stellar mass decreases to high redshift according to Figure 1(c) where the sizes appear smaller.

(± 0.1 dex) centered on the progenitor mass at a given redshift. We use this UVJ selection to identify SFGs, which occupy the bottom right portion of these diagrams (Williams et al. 2009; Patel et al. 2012). The descendants, which are more massive, become redder toward low redshift likely due to their aging stellar populations. In the SDSS sample, galaxies with SSFR $> 10^{-11}$ yr^{-1} were selected as SFGs. Figure 3 shows example SDSS *i*-band and *HST* WFC3 postage stamps for progenitor SFGs at different redshifts.

4. RESULTS

4.1. *Structural Evolution*

We examine the evolution in various structural parameters for our sample of progenitor SFGs in Figure 4. Panel (a) shows that most of the progenitors at high redshift have close to exponential profiles while those at lower redshift have slightly higher Sérsic indices. The median axis ratio in panel (b) remains relatively constant at $b/a \approx 0.60$, a low value which for a population of randomly inclined disks would imply an intrinsic axis ratio of ~ 0.2. The low Sérsic indices at higher redshifts and low axis ratios therefore point to the progenitor SFGs as being disks.

Half-light radii provide a first order view into the distribution of stellar mass for galaxies in our sample. Figure 4(c) shows the evolution of the median half-light radius with redshift. Though we follow the median of a given property, it is important to note that at a given redshift and stellar mass, SFGs display a diversity of property values. The black dashed line represents a fit to the data of the form:

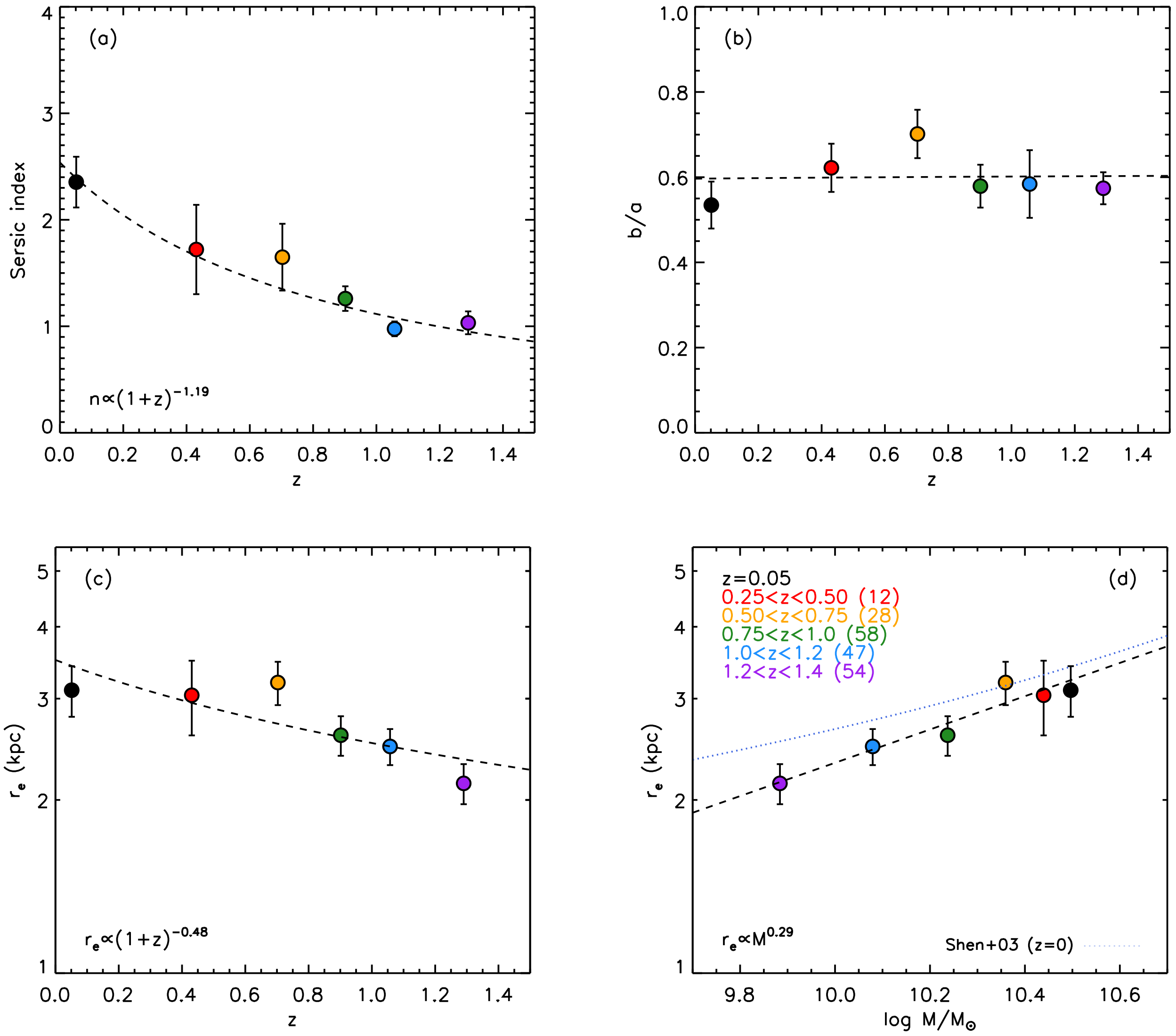

Figure 4. (a) Median Sérsic index versus redshift for progenitor SFGs. (b) Median axis ratio versus redshift. (c) Median half-light radius versus redshift. The error bars represent the bootstrapped uncertainty on the median. Fits of the form $(1+z)^\alpha$ are indicated for the Sérsic indices and half-light radii, both of which increase toward low redshift. (d) Evolution of r_e in the size-mass plane. The dotted blue line is the $z \sim 0$ SDSS size-mass relation (z-band) for late-type galaxies from Shen et al. (2003). The dashed line is a fit to the data of the form $r_e \propto M^\alpha$, where $\alpha = 0.29 \pm 0.08$. Since $z = 1$, the half-light radii of the SFGs have grown by a factor of ~ 1.4.

$$r_e = \beta(1+z)^\alpha \tag{2}$$

where $\beta = 3.5 \pm 0.3$ kpc and $\alpha = -0.48 \pm 0.15$. We note that all of the SDSS data points in Figure 4 include a 10% error added in quadrature to account for systematics between different measurement methods. Since $z = 1$, the median half-light radius for these SFGs has grown by a factor of ~ 1.4, indicative of some amount of inside-out growth.

Figure 4(d) shows the evolution of the progenitors in the size-mass plane. For reference, the SDSS $z \sim 0$ size-mass relation for late-type galaxies from Shen et al. (2003) is indicated by the dotted blue line. The dashed line represents a fit to our sample of the form:

$$r_e \propto M^\alpha \tag{3}$$

where $\alpha = 0.29 \pm 0.08$. Interestingly, the value of α measured here for SFGs is much smaller than that for QGs ($\alpha_{\rm QG} \approx 2$; van Dokkum et al. 2010; Patel et al. 2013). SFGs generally appear to evolve near the local scaling relation below $z \lesssim 1.3$, consistent with slow evolution in the zeropoint of the size-mass relation for SFGs (van der Wel et al., in prep).

4.2. *Stellar Mass Growth in the Central and Outer Regions at $z < 1.3$*

Stellar mass surface density profiles provide a detailed look at the distribution of mass within galaxies. Figure 5(a) shows the median combined mass surface density profiles for our sample of SFG progenitors. These profiles were constructed in a similar manner to that of Patel et al. (2013), where the best-fit single component Sérsic profiles were stacked to create the median light profile. A single component Sérsic profile is generally

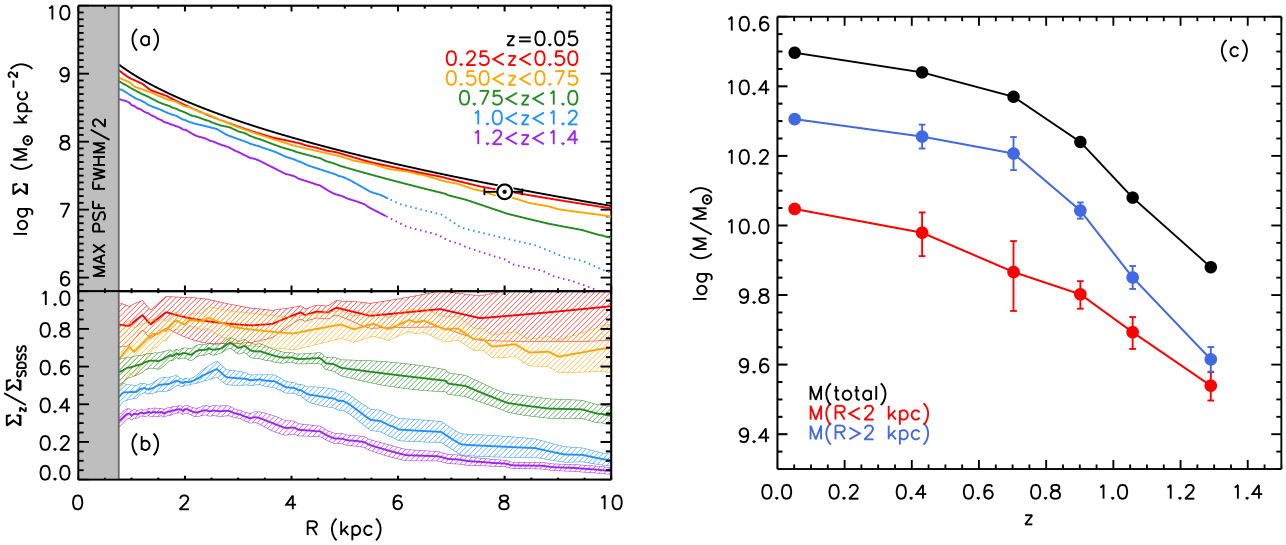

Figure 5. (a) Median combined mass surface density profiles. The dotted portion of each curve indicates where the uncertainty becomes larger than $> 20\%$. The shaded gray region indicates the maximum WFC3 PSF FWHM/2. The solar symbol indicates the mass surface density in the solar neighborhood as computed by Bovy et al. (2012) but scaled down by 0.2 dex to account for the difference in mass between the Milky Way and our $z \sim 0$ descendants. (b) The ratio of the mass profiles at higher redshifts to the SDSS mass profile. Shaded region indicates the uncertainty. The factor of 2.4 ± 0.3 mass growth from $z \sim 0.9$ to $z \sim 0$ at $R_0 = 8$ kpc agrees well with measurements in the solar neighborhood from Aumer & Binney (2009). (c) Median stellar mass growth for the central ($R < 2$ kpc, red) and outer regions ($R > 2$ kpc, blue). The total stellar mass growth is shown in black. While most of the new mass growth since $z \sim 1$ has taken place in the outer regions, mass has also been added in the central regions of these SFGs where bulges and pseudobulges are common features. Some portion of the growth in the central regions is due to star formation as Hα maps for SFGs at $z \sim 1$ are centrally peaked (Nelson et al. 2013).

found to be a good representation of the light profile for individual galaxies at high redshifts (Szomoru et al. 2012; Mosleh et al. 2013). Prior to stacking, each light profile was converted into a mass profile by normalizing the light within $R = 20$ kpc to the total stellar mass of each galaxy. While this method ignores M/L gradients, Szomoru et al. (2013) find such gradients in the rest-frame g-band to be small for higher redshift galaxies and that they do not evolve (here, we trace a redder rest-frame i-band). We plan to explore the full impact of M/L gradients in followup work. Figure 5(b) shows the ratio of the mass profiles at higher redshifts to the SDSS mass profile. Below $z \lesssim 1.3$, stellar mass is continually built up at all radii.

Figure 5(c) shows the growth in the projected mass inside (red) and outside (blue) of $R = 2$ kpc (i.e., $\approx r_e$ at $z \sim 1.3$). Clearly more mass has assembled at larger radii since $z \sim 1.3$, leading to larger r_e toward low redshift. However, the amount of stellar mass in the central regions, where bulges and pseudobulges are common structural features in nearby late-type galaxies (Weinzirl et al. 2009), has also increased. Some portion of the growth in the central regions is due to star formation as Hα maps for SFGs at $z \sim 1$ are centrally peaked (Nelson et al. 2013). This is qualitatively consistent with recent observations of stars in the Milky Way bulge that display a wide range of metallicities and ages, implying an extended formation history (Bensby et al. 2013). The ongoing mass assembly in the central regions may point to secular processes (e.g., Kormendy & Kennicutt 2004) as an important channel for bulge growth for SFGs in the stellar mass regime studied here.

5. DISCUSSION

5.1. *A Comparison with the Stellar Mass Growth in the Solar Neighborhood*

Given the significant mass assembly found at large radii, we compare our results in such a region of our galaxy that has been well documented, the solar neighborhood. Though we caution that the Milky Way is just one such SFG, and may not be one that is an archetypal late-type (Hammer et al. 2007), this analysis nevertheless provides an intriguing comparison between our lookback study and galactic archeology. The solar symbol in Figure 5(a) indicates the stellar mass surface density at the solar radius ($R_0 = 8.0$ kpc; Vanhollebeke et al. 2009) for the Milky Way from Bovy et al. (2012) but scaled down by 0.2 dex to account for the difference in mass with our descendant SFGs at $z \sim 0$. The systematic uncertainty in this correction may account for the slight offset from the SDSS mass profile, though the rough agreement is still remarkable. Aumer & Binney (2009) estimate a mean formation time for stars in the solar neighborhood that corresponds to $z \sim 0.9$. Assuming this mean is close to the median formation redshift, therefore implying a factor of ~ 2 growth below $z \lesssim 0.9$, this estimate is close to the factor of $\sim 2.4 \pm 0.3$ growth in our mass surface density from $z \sim 0.9$ (green line) to the SDSS mass profile at $R = 8$ kpc.

5.2. *Caveats*

Two caveats to the analysis presented here warrant some consideration. First, the contribution of stars formed ex situ to the stellar mass growth is an uncertain quantity, though there is evidence that it is minimal. Both Behroozi et al. (2012) and Moster et al. (2013) find that for local halos of mass $M_{\rm h} \sim 10^{12}\ M_\odot$ (hosting centrals of stellar mass $M = 10^{10.5}\ M_\odot$), little stellar mass was accreted. At the lowest redshifts, Behroozi et al. (2012) find a growing contribution, but this is likely driven by the dominance of QGs in their halos at low redshift, which primarily grow from mergers. Major mergers are likely rare in our sample at $z \lesssim 1$ as such events tend to destroy disks, contrary to what is observed at low redshift (Figure 3).

Second, the QG fraction increases toward low redshift and as a result not all SFGs at $z \sim 1.3$ will be progenitors of SFGs at low redshift as some will have quenched. This would impact our results if there is a relation between the structure of high redshift SFG progenitor candidates and low redshift QG descendants, as the former would bias our measurements for the median structural property. Exploring these caveats is beyond the scope of this Letter but will be addressed in future work.

5.3. *Conclusions*

In this Letter, we have used the evolution in the SSFR-mass relation to determine the stellar mass growth (e.g., Leitner 2012) for progenitors of SFGs like the Milky Way. We used 3D-HST redshifts and photometry to select SFGs of the appropriate progenitor mass at different redshifts back to $z \sim 1$ and *HST* CANDELS imaging to follow their structural evolution. As these SFGs grew in stellar mass by a factor of ~ 2 since $z \sim 1$, most of the new stellar mass assembled in the outer regions, leading to a factor of ~ 1.4 increase in the half-light radius. The mass surface density profiles indicate ongoing stellar mass assembly also in the central regions where bulges and pseudobulges are common features in spirals. We also found good agreement between the mass growth at $R = 8$ kpc in our lookback study and that for the solar neighborhood of the Milky Way.

REFERENCES

Aumer, M. & Binney, J. J. 2009, MNRAS, 397, 1286
Behroozi, P. S., Wechsler, R. H., & Conroy, C. 2012, arXiv:1207.6105
Bensby, T., Yee, J. C., Feltzing, S., et al. 2013, A&A, 549, A147
Blanton, M. R., Hogg, D. W., Bahcall, N. A., et al. 2003, ApJ, 594, 186
Blanton, M. R., Schlegel, D. J., Strauss, M. A., et al. 2005, AJ, 129, 2562
Bovy, J., Rix, H.-W., & Hogg, D. W. 2012, ApJ, 751, 131
Brammer, G. B., van Dokkum, P. G., & Coppi, P. 2008, ApJ, 686, 1503
Brammer, G. B., van Dokkum, P. G., Franx, M., et al. 2012, ApJS, 200, 13
Brinchmann, J., Charlot, S., White, S. D. M., et al. 2004, MNRAS, 351, 1151
Chabrier, G. 2003, PASP, 115, 763
Chomiuk, L. & Povich, M. S. 2011, AJ, 142, 197
Franx, M., van Dokkum, P. G., Schreiber, N. M. F., et al. 2008, ApJ, 688, 770
Fumagalli, M., Patel, S. G., Franx, M., et al. 2012, ApJ, 757, L22
Grogin, N. A., Kocevski, D. D., Faber, S. M., et al. 2011, ApJS, 197, 35
Guedes, J., Callegari, S., Madau, P., & Mayer, L. 2011, ApJ, 742, 76
Hammer, F., Puech, M., Chemin, L., Flores, H., & Lehnert, M. D. 2007, ApJ, 662, 322
Karim, A., Schinnerer, E., Martínez-Sansigre, A., et al. 2011, ApJ, 730, 61
Koekemoer, A. M., Faber, S. M., Ferguson, H. C., et al. 2011, ApJS, 197, 36
Kormendy, J. & Kennicutt, Jr., R. C. 2004, ARA&A, 42, 603
Kriek, M., van Dokkum, P. G., Labbé, I., et al. 2009, ApJ, 700, 221
Leitner, S. N. 2012, ApJ, 745, 149
Marchesini, D., van Dokkum, P. G., Förster Schreiber, N. M., et al. 2009, ApJ, 701, 1765
Mosleh, M., Williams, R. J., & Franx, M. 2013, arXiv:1302.6240
Moster, B. P., Naab, T., & White, S. D. M. 2013, MNRAS, 428, 3121
Nelson, E. J., van Dokkum, P. G., Momcheva, I., et al. 2013, ApJ, 763, L16
Noeske, K. G., Weiner, B. J., Faber, S. M., et al. 2007, ApJ, 660, L43
Patel, S. G., Holden, B. P., Kelson, D. D., et al. 2012, ApJ, 748, L27
Patel, S. G., van Dokkum, P. G., Franx, M., et al. 2013, ApJ, 766, 15
Peng, C. Y., Ho, L. C., Impey, C. D., & Rix, H.-W. 2002, AJ, 124, 266
Rix, H.-W. & Bovy, J. 2013, arXiv:1301.3168
Rocha-Pinto, H. J., Scalo, J., Maciel, W. J., & Flynn, C. 2000, A&A, 358, 869
Roškar, R., Debattista, V. P., Stinson, G. S., et al. 2008, ApJ, 675, L65
Salim, S., Rich, R. M., Charlot, S., et al. 2007, ApJS, 173, 267
Scannapieco, C., Wadepuhl, M., Parry, O. H., et al. 2012, MNRAS, 423, 1726
Shen, S., Mo, H. J., White, S. D. M., et al. 2003, MNRAS, 343, 978
Stinson, G. S., Brook, C., Macciò, A. V., et al. 2013, MNRAS, 428, 129
Szomoru, D., Franx, M., & van Dokkum, P. G. 2012, ApJ, 749, 121
Szomoru, D., Franx, M., van Dokkum, P. G., et al. 2013, ApJ, 763, 73
van der Wel, A., Bell, E. F., Häussler, B., et al. 2012, ApJS, 203, 24
van Dokkum, P. G., Whitaker, K. E., Brammer, G., et al. 2010, ApJ, 709, 1018
van Dokkum, P. G., et al. 2013, ApJL, submitted
Vanhollebeke, E., Groenewegen, M. A. T., & Girardi, L. 2009, A&A, 498, 95
Weinzirl, T., Jogee, S., Khochfar, S., Burkert, A., & Kormendy, J. 2009, ApJ, 696, 411
Whitaker, K. E., van Dokkum, P. G., Brammer, G., & Franx, M. 2012, ApJ, 754, L29
Williams, R. J., Quadri, R. F., Franx, M., van Dokkum, P., & Labbé, I. 2009, ApJ, 691, 1879
Wuyts, S., Förster Schreiber, N. M., Lutz, D., et al. 2011, ApJ, 738, 106